Nuclear Instruments and Methods in Physics Research A 1060 (2024) 169081

Contents lists available at ScienceDirect

Nuclear Inst. and Methods in Physics Research, A

journal homepage: www.elsevier.com/locate/nima

Full Length Article

Evaluation of vertical alignment in carbon nanotubes: A quantitative approach

Ravi Prakash Yadav [a,b,*], Ilaria Rago [a,b], Francesco Pandolfi [b], Carlo Mariani [a,b], Alessandro Ruocco [c], Sammar Tayyab [a,b], Alice Apponi [c], Gianluca Cavoto [a,b]

[a] Department of Physics, Sapienza University of Rome, Piazzale Aldo Moro, 5, Rome, 00185, Lazio, Italy
[b] INFN Sezione di Roma, Piazzale Aldo Moro, 5, Rome, 00185, Lazio, Italy
[c] Dipartimento di Scienze, Universitá Degli Studi Roma Tre and INFN Sezione di Roma Tre, Via della Vasca Navale 84, Rome, 00146, Lazio, Italy

ARTICLE INFO

Keywords:
Vertically aligned carbon nanotubes
Plasma enhanced chemical vapor deposition (PECVD)
Coherency
SEM

ABSTRACT

An automated quantitative study of the alignment of vertically aligned carbon nanotubes (VA-CNTs) from scanning electron microscopy (SEM) images has been demonstrated. It is based on the fact that the image gradient (directional change in intensity or color) at every pixel in the image contains the information about the anisotropy at that particular pixel i.e., the local alignment is maintained in the orthogonal direction to the gradient. Structure tensor metrics are formulated demonstrating to be able to summarize the distribution of gradient directions within the neighborhood of any pixel within a two-dimensional domain (surface). An image analysis is presented that evaluates the alignment in desired regions of interest (ROIs) in SEM images of VA-CNTs. This method has been exploited to study the alignment of two different kinds of VA-CNTs: one grown via the thermal chemical vapor deposition (T-CVD) method and the second synthesized via the plasma enhanced chemical vapor deposition (PE-CVD) method.

1. Introduction

Nanostructures with dimensionality one have gained significant research interest for various applications like in field emission [1,2], accelerometers [3], gas sensors [4], electrochemical biosensors [5], quantum wires [6,7] and aerospace materials [8], etc. Depending on the application, a very precise level of perfection at the nanoscale is required in terms of length, diameter, aspect ratio, and morphology [9,10]. Carbon nanotubes (CNTs) are one of those important 1-D materials which are used in various applications. Our research project, ANDROMeDa (Aligned Nanotube Detector for Research On MeV Dark-matter) aims to explore CNTs in the field of particle detectors, by developing a novel dark matter detector: the Dark-PMT [11]. The Dark-PMT is composed of a cathode made of VA-CNTs which serves as the target for dark matter [12], and an anode equipped with a solid-state detector dedicated to measuring electrons emitted by the cathode [13]. Dark matter particles from the wind would interact within the carbon nanotubes and eject electrons from the carbon lattice. As vertically aligned nanotubes have much lower density in the direction of the tubes, the ejected electrons would be able to leave the target, without being reabsorbed, if they travel in the direction of the tubes, which would happen most often when the tubes are pointing in the direction of Cygnus. NanoUV is another project in which we propose a novel concept of ultra-violet (UV) light detector that will be more compact and therefore portable with improved sensitivity. In this, we will use photocathode made of VA-CNTs to emit electrons through the photo-electric effect after absorbing the UV light, and silicon electron counter to detect these emitted electrons.

The revolutionary step lies in the use of VA-CNTs as photocathode, which are graphene sheets wrapped in the cylindrical form having diameter in the range of few nanometres (nm) [14]. VA-CNTs have close to vanishing density in the tube axis direction which allows to minimize photoelectron reabsorption in the photocathode. In this work, the catalytic CVD technique is exploited for the synthesis of VA-CNTs, it is the most widely used process for the synthesis of VA-CNTs [14,15]. In this process, hydrocarbon gas (carbon precursor) is decomposed at high temperatures and allowed to interact with a solid substrate covered with catalyst particles (Fe, Co, Ni nanoparticles), which results in the formation of vertically oriented CNTs. In CVD synthesis, the tube morphology and structural properties are dictated by both catalyst characteristics (i.e., type, size, and density) and process parameters (i.e., growth temperature, reaction pressure and time, and gas composition and flowrate) [16,17]. The synchronous synthesis of CNTs with different growth rates leads to the wavy structure at nanoscale [18].

* Corresponding author at: Department of Physics, Sapienza University of Rome, Piazzale Aldo Moro, 5, Rome, 00185, Lazio, Italy.
E-mail addresses: raviprakash.yadav@uniroma1.it (R.P. Yadav), gianluca.cavoto@uniroma1.it (G. Cavoto).

https://doi.org/10.1016/j.nima.2024.169081
Received 31 October 2023; Received in revised form 24 December 2023; Accepted 4 January 2024
Available online 6 January 2024

For the above-mentioned applications and similar applications like field emission, it is very important to have perfect alignment of CNTs in the vertical direction to minimize the reabsorption of photoelectrons.

For this purpose, it is very crucial to monitor and evaluate the alignment of CNTs simultaneously with the synthesis procedure to improve it. Although SEM is a widely used technique to examine the morphology of CNTs, an image analysis method is still necessary to accurately define and compare the waviness of CNTs at the nanoscale level from SEM images. Usually, the orientation of 1-D nanostructures is defined by Herman orientation factor (HOF) [19–21] which is calculated by taking the fast Fourier transform (FFT) of the SEM micrograph [22] and then evaluating the FFT intensity as a function of the angle. For a system, oriented along the desired axis the HOF is 1, for perpendicular orientation it is −0.5, and for a randomly distributed system, it is 0. However this method is not applicable for such case when there is a completely white image with a black background i.e., all the pixels in image have the same pixel intensity, which might be the case in a small region of the SEM image of VA-CNTs where the CNTs are so densely entangled into each other that there is constant pixel intensity value in that region. In the case of a uniform pixel value image, the HOF comes out to be 1, because in a way they are oriented along the desired axis even if it is an image with constant brightness or intensity. Therefore it is required to look for another parameter that can differentiate between the perfectly aligned and wavy nanostructures. In this work, we propose parameter *Coherency* (C) which can be used for defining the alignment of VACNTs. Image analysis is performed on SEM micrographs of VA-CNTs grown via thermal CVD method using software ImageJ [23] to define the waviness of VA-CNTs and, for better visualization, MATLAB has been used to plot the *Coherency* values in a heatmap. To improve the alignment, the PE-CVD method has been exploited. The image analysis has been performed on SEM images of PE-CVD grown CNTs also, to understand if the alignment has been improved or not when we compare with thermal CVD grown VA-CNTs.

2. Methods

VA-CNTs synthesis was performed at TITAN lab, Sapienza University of Rome using a customized and high-vacuum thermal CVD reactor with base pressure up to 10^{-7} mbar range, which is also equipped with a radiofrequency (RF) source (13.56 MHz) along with matching network, making it versatile to grow VA-CNTs via thermal CVD method as well as PECVD method. The thermal CVD process used for the growth for VA-CNTs is described in the previous studies [17,24–27]. Briefly, silicon p-type/Boron-doped <100> SiO_2/Si wafers were used as growth substrates. Thin layer of 3 nm iron was deposited on the Si substrates using the electron beam (E-beam) evaporation method. The Si substrates were then mounted on the graphite heating element inside the high-vacuum CVD chamber. At this point, an annealing treatment of the as-prepared growth substrate was performed in H_2 atmosphere at 720 °C for 4 minutes with flowrate of up to 320 sccm to reduce the oxide layers which might form on the Fe/SiO_2/Fe substrate during the transferring the sample from evaporation chamber to the CVD chamber because of the exposure to the atmosphere. The annealing step also helps in the de-wetting of the catalyst layer and nucleation of iron-based nanoparticles as a template for the CNT growth in further step. In the next step, the hydrocarbon gas (acetylene) is passed inside the chamber with flowrate of 300 sccm for 10 minutes at 740 °C up to a partial pressure of 50 mbar.

In the PE-CVD process, the annealing step is performed in H_2 atmosphere at 630 °C for 4 minutes with flowrate up to 320 sccm. The synthesis step is performed at 650 °C with flowrate of 18 sccm of acetylene for 10 minutes up to a partial pressure of 2 mbar, at a plasma power of 50 W. In PECVD plasma is formed by an electric field between two parallel plates that ionizes the gas in between and the energy is transferred by collision between the particles. The energy required for the chemical reactions (i.e., hydrocarbon decomposition, carbon diffusion through the catalyst nanoparticles, carbon precipitation, and crystallization in a cylindrical network) is not only provided by higher temperature but also by the collisions with high energy plasma particles [28,29]. The parameter optimization for growth was based on previous studies related to the VA-CNTs synthesis on different substrates [24–27]. After the synthesis step, the sample is allowed to cool down to room temperature under the base pressure of the CVD system.

First, after the growth, the CNTs are characterized with field emission-SEM (FE-SEM) by secondary electrons collection on Zeiss Auriga SEM (Jena, Germany) operating at accelerating voltage of 5 kV. SEM images were taken with a resolution of 1024 × 768 pixels. Image analysis software ImageJ was used to perform further image analysis on the SEM images. These images were divided into several (48) ROIs; OrientationJ [30], a Java plugin for ImageJ was used to compute the *Coherency* (C) for all the ROIs. OrientationJ works on the principle of evaluation of the structure tensor [31] in a local neighborhood [30], which provides information about the orientation and isotropic properties of ROI in an image. The structure tensor is an efficient tool to analyze low-level features like corner edge and corner detection as well as texture analysis.

In 2D, at any location $r_0(x_0, y_0)$, the structure tensor is defined by [32]

$$S(x_0, y_0) = \iint_R w(x - x_0, y - y_0)(\nabla f(x, y))\nabla^T f(x, y)dxdy$$

where $f(x, y)$ is the image function corresponding to associated pixel intensity value with each spatial coordinate in the image, and $w(x, y)$ is a weighting function (e.g., a Gaussian) centered at (x_0, y_0) such that $w(x, y) \geq 0$. $S(x_0, y_0)$ come out to be a (2×2) matrix, which can be written as

$$S(x_0, y_0) = \iint_R w(x - x_0, y - y_0) \begin{bmatrix} (f_x(x, y))^2 & (f_x(x, y))(f_y(x, y)) \\ (f_y(x, y))(f_x(x, y)) & (f_y(x, y))^2 \end{bmatrix} dxdy$$

$$S(x_0, y_0) = \begin{bmatrix} (w * f_x^2))(x_0, y_0) & (w * f_x f_y)(x_0, y_0) \\ (w * f_y f_x)(x_0, y_0) & (w * f_y^2))(x_0, y_0) \end{bmatrix}$$

this matrix is nothing but the weighted inner product of function $f(x, y)$ and its gradient $\nabla f(x, y)$, where f_x is partial derivative of f with respect to x, f_y is partial derivative of f with respect to y and $w * f$ stands for convolution of w and f.

This structure tensor has two eigen-values, λ_1 and λ_2, such that $\lambda_1 \geq \lambda_2 \geq 0$, with $\lambda_1, \lambda_2 \in R$. These eigenvalues contain information about the gradient distribution within the window w. Eigen-values and the corresponding eigenvectors contain the information about distribution of the gradient and can discriminate between the regions with rotational symmetry, homogeneity, and predominant alignment. For that purpose, two features *energy* (E) and *coherency* (C) has been defined. From on the eigenvalues of the structure tensor, the *energy* can be defined as $E = Trace(S) = \lambda_1 + \lambda_2$. If $E \approx 0$, which complies with $\lambda_1 = \lambda_2 \approx 0$, then the region is homogeneous i.e., the image has a constant or uniform intensity of all the pixels. If $E \gg 0$, then the anisotropy of the image is determined by the *coherency* (C) information, which can be defined as

$$0 \leq C = (\lambda_1 - \lambda_2)/(\lambda_1 + \lambda_2) = \sqrt{(S_{22} - S_{11})^2 + 4S_{12}^2}/(S_{22} + S_{11}) \leq 1$$

If $C \approx 0$, which complies with $\lambda_1 = \lambda_2$, then the region is isotropic in the local neighborhood and does not have any predominant direction i.e., it is rotational symmetric without any preferred orientation. If $C \approx 1$, which complies with $\lambda_1 \geq 0$, $\lambda_2 \approx 0$ or $\lambda_1 \geq \lambda_2$, the gradient is totally aligned and the local image or structure has one dominant orientation. For $0 \leq C \leq 1$, the dominant orientation stands between the gradient directions. In general, if C is closer to 1 then the structure in the image is locally 1D, if C is closer to 0 then there is no preferred orientation or direction.

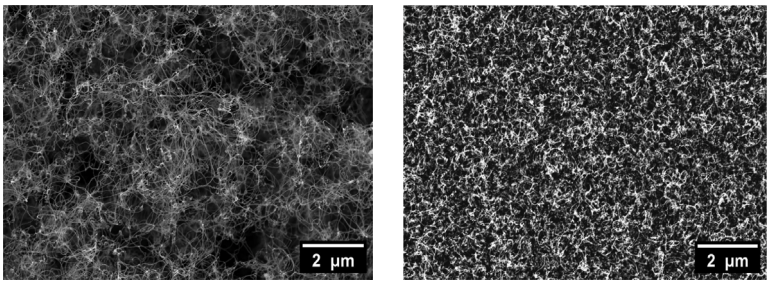

Fig. 1. Top view SEM image of VA-CNTs grown via (a) thermal CVD and (b) PECVD method respectively.

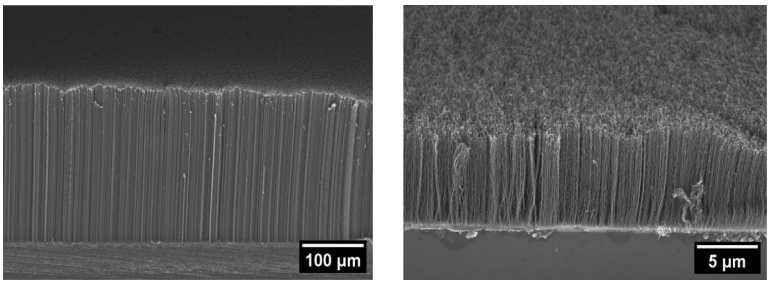

Fig. 2. Side view SEM image of VA-CNTs grown via (a) thermal CVD and (b) PECVD method, respectively.

The energy of the derivative in some direction $u_\theta = (\cos\theta, \sin\theta)$ can be written as

$$\left|\left|D_u f\right|\right|_w^2 = \langle u^T \nabla f \ , \ u^T \nabla f \rangle_w = u^T \langle \nabla f \ , \ \nabla f \rangle_w u = u^T S u$$

In the window centred around $r_0(x_0, y_0)$, the direction $u_\theta = (\cos\theta, \sin\theta)$ along which the directional derivative is maximized is given by

$$u_\theta = \arg \max_{||u||=1} \left|\left|D_u f\right|\right|_w^2$$

Here, $\left|\left|D_u f\right|\right|_w^2$ is deciphered as the average energy in the window w centred at x_0, and $D_u f$ is the directional derivative in the direction of u. The directional derivative is maximized along the eigenvector corresponding to the larger eigenvalue of the structure tensor at x_0. The direction along which the structure of the image is dominantly oriented in the local window w is given as $u_\theta = (\cos\theta, \sin\theta)$, where $\theta = 1/2 \arctan\left(2S_{12}/(S_{22} - S_{11})\right)$ [32].

'OrientationJ Dominant Direction' functionality has been used in the OrientationJ plugin, which using the principle of structure tensor gives the coherency and dominant orientation corresponding to all 48 ROIs in tabular form. These values are saved in a document file, and for better visualization, these are further arranged in the table and a heatmap (Figs. 3 and 4) is plotted for these values using MATLAB (see supplementary information). The same process is repeated for all the SEM images of VA-CNTs taken starting from top crust layer to the bottom, such that the whole vertical length of the VA-CNTs is covered. It is done for the VA-CNTs grown via thermal CVD as well as PE-CVD method (Figs. 3 and 4).

3. Results and discussion

SEM analysis was performed on the VA-CNTs grown via thermal CVD and PE-CVD method, to analyze the difference in the morphology, length, and alignment of the VA-CNTs. Fig. 1 shows the SEM images of the top view of the VA-CNTs grown via thermal CVD and PE-CVD respectively. From the top, both seem to be an arrangement of dense, entangled, and randomly oriented CNTs which are grown at the beginning of the synthesis step due to differences in the growth rate and nucleation times [33,34]. This is termed as crust layer [33] which needs to be tailored for some specific application. However from Figs. 1(a) and 1(b) it seems that the PE-CVD grown VA-CNTs are more densely packed as compared to the thermal CVD grown VA-CNTs. From Fig. 2 the main difference between these two is the length of VA-CNTs. The PE-CVD grown VA-CNTs are shorter in length (around 7.5 μm) (Fig. 2(b)), while the thermal CVD grown VA-CNTs are longer in length (around 200 μm) (Fig. 2(a)). Both the SEM micrographs (Figs. 2(a) and 2(b)) shows the full length of VA-CNTs for both cases and due to this big difference in length they are at different scale bar. A possible reason behind the large difference in length could be the flow rate with which the hydrocarbon gas is passed inside the chamber during the synthesis process. Plasma power and flowrate (i.e., partial pressure) of hydrocarbon gas were tuned to optimize the PE-CVD process. We optimized the process at a plasma power of 50 W and flowrate of 18 sccm of acetylene, which is much less as compared to that of the thermal CVD process, which is 300 sccm. This could be a possible explanation for the shorter length of PE-CVD grown VA-CNTs as compared to that of thermal CVD grown VA-CNTs [35,36].

When we look at the same magnification for both the cases (Figs. 3 and 4), the PE-CVD grown VA-CNTs show better alignment in the vertical direction as compared to thermal CVD grown VA-CNTs. In Figs. 3 and 4 the side view SEM image for both the methods has been presented; the image has been divided into 48 ROIs and for each ROI *coherency* has been calculated which is represented in the form of heatmap along with the SEM image itself. It can be visualized that the *coherency* values are closer to 1 in the case of PE-CVD grown VA-CNTs (Figs. 3(b) and 4(b)), which means the VA-CNTs are more straight and aligned in the vertical direction while in the case of thermal CVD grown VA-CNTs the coherency is comparatively lower (Figs. 3(a) and 4(a)), in the range (0.1–0.5) which corresponds to the less preferred oriented system. In the heatmap in Fig. 3(b) corresponding to PE-CVD grown VA-CNTs, the top row and the bottom row also have lower coherency values, because looking at the corresponding SEM image, the bottom part of the image includes some part of the substrate, which has a constant pixel intensity value. The top layer of the SEM image

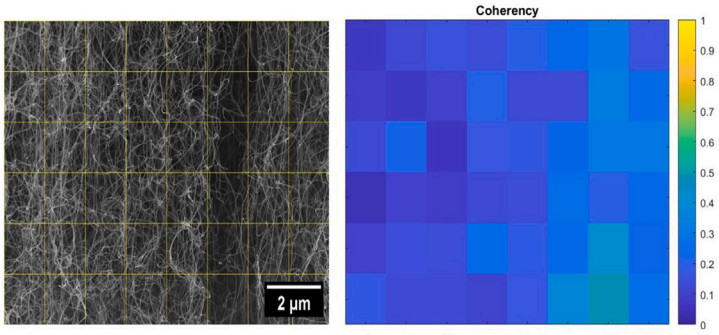

(a)

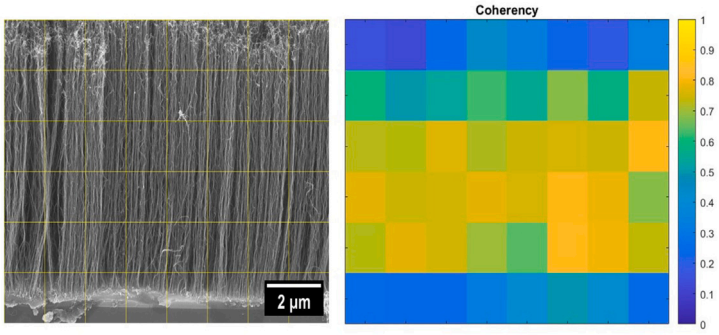

(b)

Fig. 3. Side view SEM image (at 25 K magnification) along with corresponding heatmaps representing the coherency values for different ROIs for VA-CNTs grown via (a) thermal CVD and (b) PECVD methods, respectively.

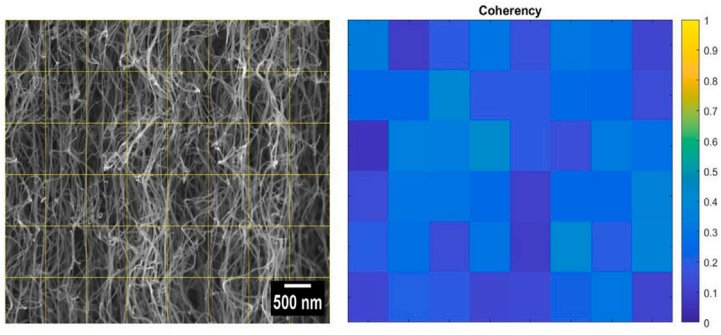

(a)

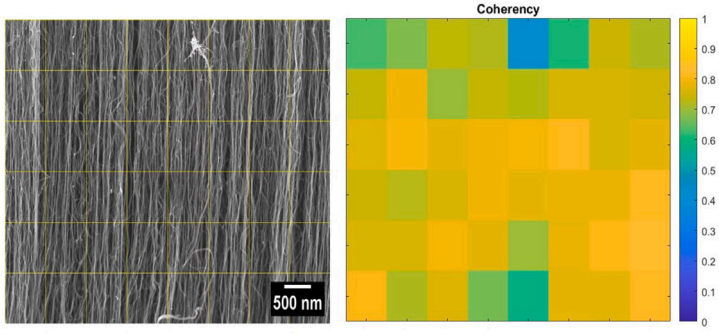

(b)

Fig. 4. Side view SEM image (at 50k magnification) along with corresponding heatmaps representing the coherency values for different ROIs for VA-CNTs grown via (a) thermal CVD method (b) PECVD method respectively.

corresponds to the top crust layer which is dense randomly oriented CNTs. Since the image is a slightly tilted view, it also contains some of the top surface of the VA-CNTs in the top row of the image, which could be also a reason why the coherency values are lower at the top. In the case of PE-CVD grown VA-CNTs, the plasma sheath electric field and high energy particles in plasma make them more reactive and facilitate their alignment along a specific direction, also resulting in low growth temperature [28,37]. It could also be a possible reason that due to comparatively lower synthesis temperatures in the PE-CVD process, there is less agglomeration and hence good dispersion and stabilization of catalyst nanoparticles, leading to more controlled and aligned growth. When catalyst particles agglomerate, there is non non-uniform distribution of catalyst nanoparticles thus allowing CNTs to orient in various orientations [18] which is a common issue in thermal CVD where the synthesis is performed at comparatively higher temperatures.

4. Conclusion

This study proposes and presents the possibility of quantifying the alignment of VA-CNTs using image processing methods and structure tensor matrix applied to the side view SEM images of VA-CNTs. We first demonstrate that uniform, highly aligned, and densely packed VA-CNTs can be successfully grown on SiO_2/Si substrate via the thermal CVD method. PE-CVD technology has been proposed as a strategy to improve the VA-CNTs' alignment. The morphological features like vertical alignment, density, and uniformity of these VA-CNTs are assessed via scanning electron microscopy. Image analysis software has been used for the SEM image analysis of the thermal CVD grown VA-CNTs and PE-CVD grown VA-CNTs respectively, and a direct comparison of alignment has been performed for both methods. The alignment has been evaluated for different ROIs in the SEM image. It has been observed that the PE-CVD grown VA-CNTs are better in terms of alignment and are less wavy than thermal CVD grown VA-CNTs. Different regions in the SEM image of PE-CVD grown VA-CNTs have a *coherency* closer to 1, while in the case of thermal CVD grown VA-CNTs, the *coherency* is closer to 0 typically in the range (0.1–0.5) which reflects less predominant orientation. This work facilitates the science community and researchers in nanoscience and nanotechnology with an automated method to determine the alignment for such applications where the dominant orientation of one-dimensional (1-D) nanostructures is required. This work can also be exploited in the field of polymer films and fibrillar collagen alignment. The alignment or arrangement of polymer chains in thin films can significantly influence the physical, mechanical, and electrical properties of the material. Controlling the alignment is crucial for tailoring the performance of polymer films in various applications [38]. While fibrillar collagen alignment refers to the ordered arrangement of collagen fibers in a tissue or extracellular matrix. The alignment of collagen fibers plays a significant role in determining the mechanical properties and functionality of these tissues. Changes in collagen alignment can be associated with various pathological conditions and diseases like breast, ovarian, kidney, and pancreatic cancers [39,40].

CRediT authorship contribution statement

Ravi Prakash Yadav: Conceptualization, Methodology, Software, Writing – original draft, Writing – review & editing. **Ilaria Rago:** Investigation, Writing – review & editing. **Francesco Pandolfi:** Investigation, Writing – review & editing, Funding acquisition. **Carlo Mariani:** Writing – review & editing, Validation. **Alessandro Ruocco:** Writing – review & editing, Validation. **Sammar Tayyab:** Writing – review & editing. **Alice Apponi:** Writing – review & editing. **Gianluca Cavoto:** Writing – review & editing, Conceptualization, Methodology, Funding acquisition, Project administration.

Declaration of competing interest

The authors declare that they have no known competing financial interests or personal relationships that could have appeared to influence the work reported in this paper.

Data availability

Data will be made available on request.

Acknowledgments

The work was supported by ATTRACT project funded by the EC under Grant Agreement 777222. Additional funding was provided by project 2020Y2JMP5 'ANDROMeDa' (CUP: I85F21004170005) funded by MUR.

Appendix A. Supplementary data

Supplementary material related to this article can be found online at https://doi.org/10.1016/j.nima.2024.169081.

References

[1] T. Zhai, L. Li, Y. Ma, M. Liao, X. Wang, X. Fang, J. Yao, Y. Bando, D. Golberg, One-dimensional inorganic nanostructures: synthesis, field-emission and photodetection, Chem. Soc. Rev. 40 (5) (2011) 2986–3004.
[2] J.-H. Deng, L.-N. Deng, R.-N. Liu, A.-L. Han, D.-J. Li, G.-A. Cheng, Vapor–solid preparation of densely distributed and small-sized graphene nanoflakes on one-dimensional nanomaterials for low-field and highly stable field emission, Carbon 102 (2016) 1–9.
[3] A. Koka, H.A. Sodano, High-sensitivity accelerometer composed of ultra-long vertically aligned barium titanate nanowire arrays, Nature Commun. 4 (1) (2013) 2682.
[4] X. Chen, C.K. Wong, C.A. Yuan, G. Zhang, Nanowire-based gas sensors, Sensors Actuators B 177 (2013) 178–195.
[5] U. Yogeswaran, S.-M. Chen, A review on the electrochemical sensors and biosensors composed of nanowires as sensing material, Sensors 8 (1) (2008) 290–313.
[6] N. Wang, Y. Cai, R. Zhang, Growth of nanowires, Mater. Sci. Eng. R 60 (1–6) (2008) 1–51.
[7] H. Yu, J. Li, R.A. Loomis, P.C. Gibbons, Wang, W.E. Buhro, Cadmium selenide quantum wires and the transition from 3D to 2D confinement, J. Am. Chem. Soc. 125 (52) (2003) 16168–16169.
[8] M. Regi, Synthesis, characterization and application of carbon nanotubes: the case of aerospace engineering, in: Nanofibers and Nanotechnology in Textiles, Elsevier, 2007, pp. 113–193.
[9] B.K. Gupta, G. Kedawat, A.K. Gangwar, K. Nagpal, P.K. Kashyap, S. Srivastava, S. Singh, P. Kumar, S.R. Suryawanshi, D.M. Seo, et al., High-performance field emission device utilizing vertically aligned carbon nanotubes-based pillar architectures, AIP Adv. 8 (1) (2018).
[10] P. Tripathi, B.K. Gupta, A. Bhatnagar, C. Patel, P.K. Banker, D.J. Late, M.A. More, N. Lalla, D. Phase, R. Choudhary, et al., Highly efficient field emission properties of radially aligned carbon nanotubes, J. Mater. Chem. C 6 (24) (2018) 6584–6590.
[11] F. Pandolfi, A. Apponi, G. Cavoto, C. Mariani, I. Rago, A. Ruocco, The dark-PMT: a novel directional light dark matter detector based on vertically-aligned carbon nanotubes, in: Journal of Physics: Conference Series, Vol. 2156, No, IOP Publishing, 2021, 012051.
[12] G. Cavoto, F. Luchetta, A. Polosa, Sub-GeV dark matter detection with electron recoils in carbon nanotubes, Phys. Lett. B 776 (2018) 338–344.
[13] A. Apponi, G. Cavoto, M. Iannone, C. Mariani, F. Pandolfi, D. Paoloni, I. Rago, A. Ruocco, Response of windowless silicon avalanche photo-diodes to electrons in the 90–900 eV range, J. Instrum. 15 (11) (2020) P11015.
[14] M. Kumar, Y. Ando, Chemical vapor deposition of carbon nanotubes: a review on growth mechanism and mass production, J. Nanosci. Nanotechnol. 10 (6) (2010) 3739–3758.
[15] X.-D. Wang, K. Vinodgopal, G.-P. Dai, Synthesis of carbon nanotubes by catalytic chemical vapor deposition, Perspect. Carbon Nanotubes (2019) 1–19.
[16] P. Sharma, V. Pavelyev, S. Kumar, P. Mishra, S. Islam, N. Tripathi, Analysis on the synthesis of vertically aligned carbon nanotubes: growth mechanism and techniques, J. Mater. Sci., Mater. Electron. 31 (2020) 4399–4443.
[17] E. Schifano, G. Cavoto, F. Pandolfi, G. Pettinari, A. Apponi, A. Ruocco, D. Uccelletti, I. Rago, Plasma-etched vertically aligned CNTs with enhanced antibacterial power, Nanomaterials 13 (6) (2023) 1081.

[18] Q. Zhang, W. Zhou, W. Qian, R. Xiang, J. Huang, D. Wang, F. Wei, Synchronous growth of vertically aligned carbon nanotubes with pristine stress in the heterogeneous catalysis process, J. Phys. Chem. C 111 (40) (2007) 14638–14643.
[19] J. Carpena-Núñez, J.A. Boscoboinik, S. Saber, R. Rao, J.-Q. Zhong, M.R. Maschmann, P.R. Kidambi, N.T. Dee, D.N. Zakharov, A.J. Hart, et al., Isolating the roles of hydrogen exposure and trace carbon contamination on the formation of active catalyst populations for carbon nanotube growth, ACS Nano 13 (8) (2019) 8736–8748.
[20] A. Mikhalchan, T. Gspann, A. Windle, Aligned carbon nanotube–epoxy composites: the effect of nanotube organization on strength, stiffness, and toughness, J. Mater. Sci. 51 (2016) 10005–10025.
[21] E. Brandley, E.S. Greenhalgh, M.S. Shaffer, Q. Li, Mapping carbon nanotube orientation by fast fourier transform of scanning electron micrographs, Carbon 137 (2018) 78–87.
[22] C. Ayres, G.L. Bowlin, S.C. Henderson, L. Taylor, J. Shultz, J. Alexander, T.A. Telemeco, D.G. Simpson, Modulation of anisotropy in electrospun tissue-engineering scaffolds: Analysis of fiber alignment by the fast Fourier transform, Biomaterials 27 (32) (2006) 5524–5534.
[23] C.A. Schneider, W.S. Rasband, K.W. Eliceiri, NIH image to ImageJ: 25 years of image analysis, Nat. Methods 9 (7) (2012) 671–675.
[24] I. Rago, R. Rauti, M. Bevilacqua, I. Calaresu, A. Pozzato, M. Cibinel, M. Dalmiglio, C. Tavagnacco, A. Goldoni, D. Scaini, Carbon nanotubes, directly grown on supporting surfaces, improve neuronal activity in hippocampal neuronal networks, Adv. Biosyst. 3 (5) (2019) 1800286.
[25] N.P. Pampaloni, I. Rago, I. Calaresu, L. Cozzarini, L. Casalis, A. Goldoni, L. Ballerini, D. Scaini, Transparent carbon nanotubes promote the outgrowth of enthorino-dentate projections in lesioned organ slice cultures, Dev. Neurobiol. 80 (9–10) (2020) 316–331.
[26] L.S. Ulloa, F. Perissinotto, I. Rago, A. Goldoni, R. Santoro, M. Pesce, L. Casalis, D. Scaini, Carbon nanotubes substrates alleviate pro-calcific evolution in porcine valve interstitial cells, Nanomaterials 11 (10) (2021) 2724.
[27] F. Sarasini, J. Tirillò, M. Lilli, M.P. Bracciale, P.E. Vullum, F. Berto, G. De Bellis, A. Tamburrano, G. Cavoto, F. Pandolfi, et al., Highly aligned growth of carbon nanotube forests with in-situ catalyst generation: A route to multifunctional basalt fibres, Composites B 243 (2022) 110136.
[28] U. Sharma, S.C. Sharma, A parametric study to unravel the alignment mechanism of carbon nanotubes during its plasma-assisted growth, Phys. Plasmas 25 (10) (2018).
[29] H. Wang, J.J. Moore, Different growth mechanisms of vertical carbon nanotubes by rf-or dc-plasma enhanced chemical vapor deposition at low temperature, J. Vacuum Sci. Technol. B Nanotechnol. Microelectron. Mater. Process. Meas. Phenomena 28 (6) (2010) 1081–1085.
[30] R. Rezakhaniha, A. Agianniotis, J.T.C. Schrauwen, A. Griffa, D. Sage, C.v. Bouten, F. Van De Vosse, M. Unser, N. Stergiopulos, Experimental investigation of collagen waviness and orientation in the arterial adventitia using confocal laser scanning microscopy, Biomech. Model. Mechanobiol. 11 (2012) 461–473.
[31] B. Jähne, Spatio-Temporal Image Processing: Theory and Scientific Applications, Springer, 1993.
[32] Z. Püspöki, M. Storath, D. Sage, M. Unser, Transforms and operators for directional bioimage analysis: a survey, Focus Bio-Image Inform. (2016) 69–93.
[33] S. Seo, S. Kim, S. Yamamoto, K. Cui, T. Kodama, J. Shiomi, T. Inoue, S. Chiashi, S. Maruyama, A.J. Hart, Tailoring the surface morphology of carbon nanotube forests by plasma etching: A parametric study, Carbon 180 (2021) 204–214.
[34] Y. Won, Y. Gao, M.A. Panzer, R. Xiang, S. Maruyama, T.W. Kenny, W. Cai, K.E. Goodson, Zipping, entanglement, and the elastic modulus of aligned single-walled carbon nanotube films, Proc. Natl. Acad. Sci. 110 (51) (2013) 20426–20430.
[35] S. Shukrullah, N. Mohamed, M. Shaharun, M. Naz, Effect of ethylene flow rate and CVD process time on diameter distribution of MWCNTs, Mater. Manuf. Process. 31 (12) (2016) 1537–1542.
[36] V. Sivamaran, V. Balasubramanian, M. Gopalakrishnan, V. Viswabaskaran, A. Gourav Rao, S. Selvamani, Carbon nanotubes, nanorings, and nanospheres: Synthesis and fabrication via chemical vapor deposition—a review, Nanomater. Nanotechnol. 12 (2022) 18479804221079495.
[37] C. Bower, W. Zhu, S. Jin, O. Zhou, Plasma-induced alignment of carbon nanotubes, Appl. Phys. Lett. 77 (6) (2000) 830–832.
[38] N.E. Persson, J. Rafshoon, K. Naghshpour, T. Fast, P.-H. Chu, M. McBride, B. Risteen, M. Grover, E. Reichmanis, High-throughput image analysis of fibrillar materials: a case study on polymer nanofiber packing, alignment, and defects in organic field effect transistors, ACS Appl. Mater. Interfaces 9 (41) (2017) 36090–36102.
[39] Y. Liu, A. Keikhosravi, G.S. Mehta, C.R. Drifka, K.W. Eliceiri, Methods for quantifying fibrillar collagen alignment, Fibrosis: Methods Protocols (2017) 429–451.
[40] Y. Liu, K.W. Eliceiri, Quantifying fibrillar collagen organization with curvelet transform-based tools, JoVE (J. Visualized Experiments) (165) (2020) e61931.